crystals

MDPI

Article

Tuning Charge Order in $(TMTTF)_2X$ by Partial Anion Substitution

Andrej Pustogow [1,2,*], Daniel Dizdarevic [1], Sebastian Erfort [1], Olga Iakutkina [1], Valentino Merkl [1], Gabriele Untereiner [1] and Martin Dressel [1,*]

[1] 1. Physikalisches Institut, Universität Stuttgart, Pfaffenwaldring 57, 70569 Stuttgart, Germany; danieldizdarevic@gmx.de (D.D.); erfort@theochem.uni-stuttgart.de (S.E.); olga.iakutkina@pi1.uni-stuttgart.de (O.I.); valentino.merkl@pi1.uni-stuttgart.de (V.M.); gabriele.untereiner@pi1.physik.uni-stuttgart.de (G.U.)

[2] Institute of Solid State Physics, TU Wien, 1040 Vienna, Austria

* Correspondence: pustogow@ifp.tuwien.ac.at (A.P.); dressel@pi1.physik.uni-stuttgart.de (M.D.)

Abstract: In the quasi-one-dimensional $(TMTTF)_2X$ compounds with effectively quarter-filled bands, electronic charge order is stabilized from the delicate interplay of Coulomb repulsion and electronic bandwidth. The correlation strength is commonly tuned by physical pressure or chemical substitution with stoichiometric ratios of anions and cations. Here, we investigate the charge-ordered state through partial substitution of the anions in $(TMTTF)_2[AsF_6]_{1-x}[SbF_6]_x$ with $x \approx 0.3$, determined from the intensity of infrared vibrations, which is sufficient to suppress the spin-Peierls state. Our dc transport experiments reveal a transition temperature T_{CO} = 120 K and charge gap $\Delta_{CO} = 430$ K between the values of the two parent compounds $(TMTTF)_2AsF_6$ and $(TMTTF)_2SbF_6$. Upon plotting the two parameters for different $(TMTTF)_2X$, we find a universal relationship between T_{CO} and Δ_{CO} yielding that the energy gap vanishes for transition temperatures $T_{CO} \leq 60$ K. While these quantities indicate that the macroscopic correlation strength is continuously tuned, our vibrational spectroscopy results probing the local charge disproportionation suggest that 2δ is modulated on a microscopic level.

Keywords: charge-transfer salts; $(TMTTF)_2X$; Fabre salts; charge order; strongly correlated electron systems; extended Hubbard model; bandwidth tuning; partial chemical substitution; negative chemical pressure; phase transitions; metal-insulator transitions; optical conductivity; vibrational spectroscopy; FTIR

PACS: 71.30.+h; 78.30.Jw; 75.25.Dk

Citation: Pustogow, A.; Dizdarevic, D.; Erfort, S.; Iakutkina, O.; Merkl, V.; Untereiner, G.; Dressel, M. Tuning Charge Order in $(TMTTF)_2X$ by Partial Anion Substitution. *Crystals* **2021**, *11*, 1545. https://doi.org/10.3390/cryst11121545

Academic Editor: Sergiy Rosokha

Received: 15 October 2021
Accepted: 4 December 2021
Published: 10 December 2021

1. Introduction

Organic charge-transfer salts are model systems realizing electronic correlations and Mott–Hubbard physics, yielding a plethora of metal–insulator transitions in many different compounds. Owing to their effectively quarter-filled bands with nominally one electron per two organic molecules, the quasi-one-dimensional Fabre salts $(TMTTF)_2X$ are prone to charge-order instabilities [1]. Initially, charge order (CO) was suggested as a purely electronic effect due to intersite Coulomb repulsion. Within the extended Hubbard model, the ratio of nearest neighbor interaction V with respect to the bandwidth W is a measure of the correlation strength that can be varied by external pressure or by chemical means [2,3]. Eventually, CO is suppressed completely for sufficiently small V/W, and an insulator–metal transition takes place, stabilizing metallic and superconducting states. At lower temperatures, more complex phase transitions to anion-ordered and spin-Peierls phases result in modifications of the magnetic and structural degrees of freedom, such as the formation of a spin gap and tetramerization of the TMTTF molecules. Previous NMR and optical studies of electronically-driven charge order provided consistent results on $(TMTTF)_2X$ with centrosymmetric anions $X = PF_6^-$, AsF_6^-, SbF_6^-, and TaF_6^- [1,4–13] and tetrahedral anions $X = BF_4^-$, ReO_4^- [14,15].

The wave function overlap $t \propto W$ and, hence, V/W, can be modified by changing the lattice parameter through introduction of bigger or smaller anions, or by the use of organic donor molecules with Se instead of S. Chemical substitution in a stoichiometric manner allows reaching distinct regions in the phase diagram, with a step size determined by the chemical properties of the respective molecules. Physical pressure, on the other hand, enables tuning in arbitrary steps through the phase diagram, at the cost of more difficult experiments that have to be carried out in a pressure cell. The advantages of both approaches—flexible tuning and ambient pressure experiments—can be achieved by partial substitution of the constituents, either the donor molecules [16–29] or the anions [30–33], as depicted in Figure 1. So far, partial substitution has remained poorly investigated compared to pressure tuning, but, in addition to bandwidth tuning, it also enables the study of disorder effects on metal–insulator transitions and superconductivity [29].

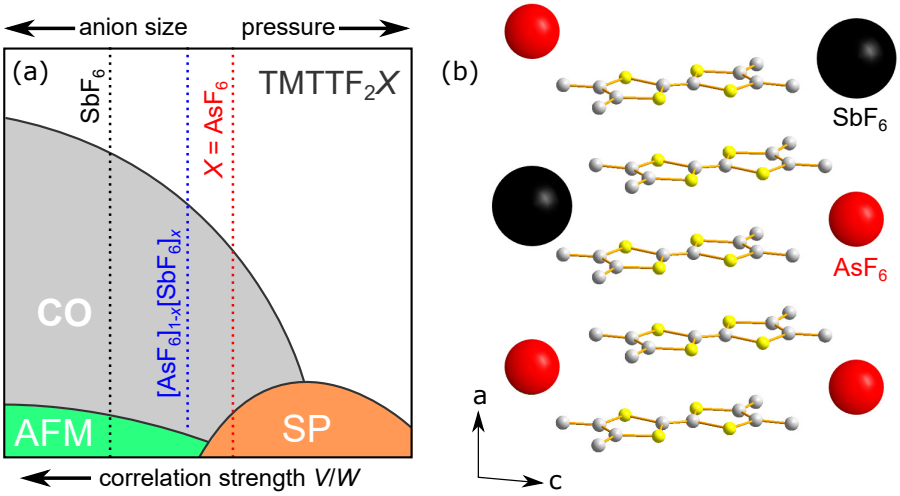

Figure 1. (Color online) (**a**) $(TMTTF)_2X$ with $X = SbF_6$ exhibits larger electronic correlation strength V/W as the molecules are separated further apart than for $X = AsF_6$. Modifying the intersite spacing via physical pressure or chemical substitution allows tuning through charge-ordered (CO), antiferromagnetic (AFM), and spin-Peierls (SP) states in the phase diagram. (**b**) Partial substitution of AsF_6 anions (red) with larger SbF_6 (black) in $(TMTTF)_2[AsF_6]_{1-x}[SbF_6]_x$ yields a position between the two parent compounds, indicated by the dotted blue line in (**a**).

Here, we investigate charge order upon partial substitution of the anions in $(TMTTF)_2[AsF_6]_{1-x}[SbF_6]_x$. The stoichiometry $x \approx 0.3$ is determined via the intensity of SbF_6^- and AsF_6^- vibration modes at 660 and 700 cm^{-1}, respectively. The lack of tetramerization and a spin gap deduced from optical and magnetic susceptibility measurements indicates the absence of a spin-Peierls state. Our dc transport results yield a transition temperature $T_{CO} = 120$ K and a charge gap $\Delta_{CO} = 430$ K. These values line up with CO in the stoichiometric $(TMTTF)_2X$ compounds, revealing that $\Delta_{CO} \to 0$ around $T_{CO} \approx 60$ K. Consistent with the resistivity data, our optical experiments on TMTTF vibrations in the infrared range yield a splitting of the charge-sensitive ν_{28} mode below T_{CO}. Despite the higher transition temperature, the charge disproportionation $2\delta = 0.21e$ (in the limit $T \to 0$) is similar to $(TMTTF)_2AsF_6$. Our findings indicate that the local amplitude of charge imbalance is linked closely to the nearest anions, while T_{CO} and Δ_{CO} are determined by the macroscopic mixture. This motivates more systematic studies of the role of the anions and the microscopic properties of CO via partial chemical substitution.

2. Materials and Experiments

CO in $(TMTTF)_2X$ has been comprehensively studied in the stoichiometric compounds with octahedral and tetrahedral anions [1,4–15]. For the former, larger anion size $d(TaF_6^-) > d(SbF_6^-) > d(AsF_6^-) > d(PF_6^-)$ yields a bigger separation of the TMTTF

molecules and, hence, an increase of electronic correlations V/W as the wave function overlap $t \propto W$ is reduced more strongly than the intersite Coulomb repulsion V (Figure 1a). This trend has been continued with the recently synthesized new member with NbF_6^- as counterion, which has similar T_{CO} as $(TMTTF)_2SbF_6$ [34]. Accordingly, the compounds with largest (smallest) anions have the highest (lowest) T_{CO}. Vice versa, physical pressure reduces the intermolecular distances, decreasing V/W and suppressing CO. However, the use of stoichiometric compounds confines the available phase space to a few distinct positions where suitable anions for single crystal growth are available. Reaching the regions in between two compounds, e.g., between $(TMTTF)_2SbF_6$ and $(TMTTF)_2AsF_6$, requires pressure tuning starting from the material with the larger anion, here SbF_6^- [1,6,35,36]; increasing V/W in small increments from the position of $X = AsF_6^-$ was not achieved so far. In principle, this region in the phase diagram could be reached by "negative" pressure which can be obtained by uniaxially applying tensile strain, but not through hydrostatic pressure.

Here, we perform continuous correlation tuning via partial chemical substitution in $(TMTTF)_2[AsF_6]_{1-x}[SbF_6]_x$. Single crystals were prepared following the standard electrochemical synthesis procedures [37]. While a mixture of approximately 1:1 SbF_6^- and AsF_6^- anions was used, the real stoichiometry upon crystallization can differ from this ratio. We determined the composition as $x \approx 0.3$ by comparing the infrared intensities of the respective anion vibration modes at 660 and 700 cm^{-1} in Figure 2. The position in the phase diagram in Figure 1a is further substantiated by measurements of the magnetic susceptibility. Our SQUID data in Figure 3 provide solid evidence that $(TMTTF)_2[AsF_6]_{1-x}[SbF_6]_x$ studied here does not exhibit a spin-Peierls ground state, because it lacks a pronounced drop of χ_s that would indicate a spin-singlet formation as in the case of $(TMTTF)_2AsF_6$ [7]. The data quality at the lowest temperatures prevents the assignment of a possible antiferromagnetic transition, which occurs at $T_N = 8$ K for $(TMTTF)_2SbF_6$ [6,35]. Further characterization of the magnetic ground state is a task for future investigations.

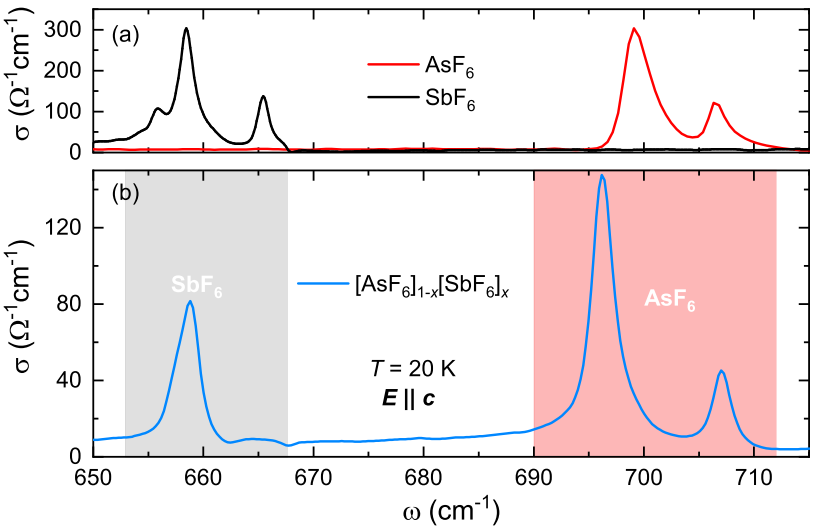

Figure 2. (**a**) The vibration modes of the anions SbF_6^- and AsF_6^- occur in the infrared spectra of $(TMTTF)_2SbF_6$ and $(TMTTF)_2AsF_6$ around 660 and 700 cm^{-1}, respectively. (**b**) The spectral features of both anion species are present in the spectrum of $(TMTTF)_2[AsF_6]_{1-x}[SbF_6]_x$. Through integrating the spectral weight SW in the grey and red shaded frequency ranges, we estimate a stoichiometry $x = 0.3$ from the ratios between the intensities of the SbF_6^- and AsF_6^- modes.

Standard optical spectroscopic experiments in the mid-infrared range (500–8000 cm^{-1}) were performed with the light polarized along the a, b, and c crystallographic axes in a temperature range from 300 K down to 5 K. We focused on evaluation of the charge-sensitive infrared active $\nu_{28}(b_{1u})$ mode probed for $E \parallel c$, the resonance frequency of which follows [1,38]

$$\nu_{28}(\rho) = 1632\ \mathrm{cm}^{-1} - \rho \cdot 80\ \mathrm{cm}^{-1}/e, \quad (1)$$

where ρ is the molecular charge and e the charge of an electron. For a characterization of the conduction properties, plotted in Figure 4a, we measured the dc resistivity in situ during the optical experiments, revealing a considerable increase of $T_{CO} = 120$ K from the transition temperature of $(TMTTF)_2AsF_6$ ($T_{CO} = 102$ K) towards that of $(TMTTF)_2SbF_6$ ($T_{CO} = 156$ K).

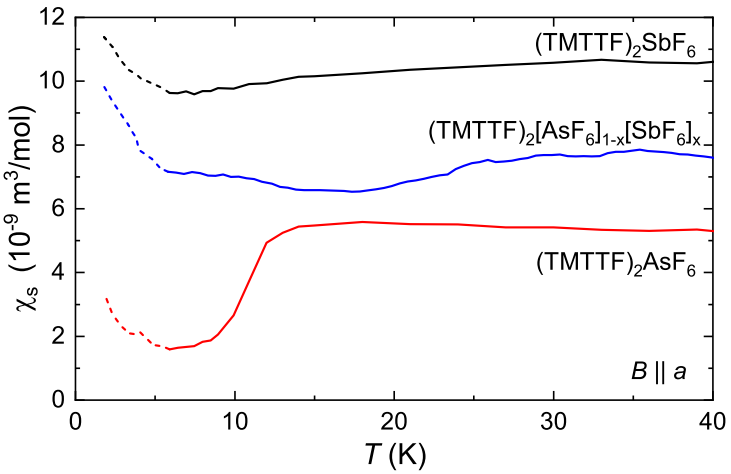

Figure 3. Temperature dependence of the magnetic susceptibility $\chi_s(T)$ for $(TMTTF)_2X$ with $X = SbF_6$, $[AsF_6]_{1-x}[SbF_6]_x$ ($x = 0.3$) and AsF_6 measured by a SQUID magnetometer. In all cases, the pronounced Curie tail below 6 K has not been subtracted (dashed region). The magnetic field was $B = 0.5$ T for the alloy and 1 T for the two pure compounds; the single crystals are oriented with $B \parallel a$. The curves of $X = SbF_6$ and $[AsF_6]_{1-x}[SbF_6]_x$ are vertically shifted by a positive offset for clarity reasons. The spin-Peierls transition in $(TMTTF)_2AsF_6$ can be clearly seen at $T_{SP} = 13$ K, whereas the antiferromagnetic transition at $T_N = 8$ K is barely visible for $(TMTTF)_2SbF_6$. For the alloy $(TMTTF)_2[AsF_6]_{1-x}[SbF_6]_x$, we cannot identify any transition within the accessible temperature range ($T > 1.8$ K).

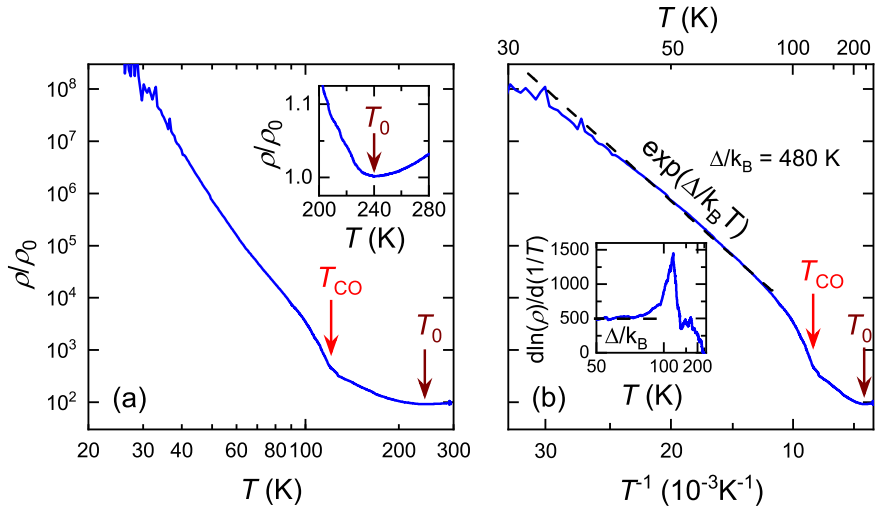

Figure 4. (**a**) Temperature-dependent electrical resistivity of $(TMTTF)_2[AsF_6]_{1-x}[SbF_6]_x$ with $x = 0.3$ (electrical current parallel to a-axis) measured in situ during optical reflection measurements in the ac-plane. The sharp increase at $T_{CO} = 120$ K indicates the CO transition. The localization temperature $T_0 = 240$ K is a little lower compared to the parent compounds $(TMTTF)_2AsF_6$ and $(TMTTF)_2SbF_6$ [37], but otherwise the transport properties are qualitatively similar. (**b**) The Arrhenius plot yields an approximately constant energy gap $\Delta/k_B = 480$ K in the temperature range 40–100 K, as illustrated in the transport derivative $d \ln \rho / d(1/T)$ in the inset.

3. Results and Analysis

The transition temperature $T_{CO} = 120$ K agrees with our expectations based on the stoichiometry, placing $(TMTTF)_2[AsF_6]_{1-x}[SbF_6]_x$ with $x = 0.3$ closer to $(TMTTF)_2AsF_6$ than to $(TMTTF)_2SbF_6$. Our comprehensive set of experimental results allows us to gain much deeper insight by evaluating distinctive quantities such as the energy gap associated with CO, as well as the charge disproportionation 2δ. In order to extract the transport gap, we plot the resistivity in an Arrhenius plot in Figure 4b. We find an approximately constant $\Delta/k_B = 480$ K between 40–100 K which is, again, in line with the gap size of the parent compounds [37]. The inset, showing the transport derivative $d \ln \rho / d(1/T)$, consistently yields a temperature-independent transport gap below the sharp peak that occurs in the vicinity of T_{CO}.

3.1. Universal Relation between Charge Gap and Transition Temperature

The bare value of the transport gap, however, does not reflect the CO state only, but involves also contributions from Mott localization that cause the upturn of resistivity below T_0. These individual contributions add in quadrature establishing the total value of $\Delta(T)$. To that end, we determine the CO contribution from the temperature-dependent energy gap $\Delta(T) = T \ln \rho$, following the procedure applied in [37]. $\Delta(T)$ of $(TMTTF)_2[AsF_6]_{0.7}[SbF_6]_{0.3}$ is shown in Figure 5a, together with the energy gaps of $(TMTTF)_2X$ with $X = PF_6^-$ (here we show the deuterated compound with T_{CO}= 90 K from [39]), AsF_6^-, and SbF_6^- [37]. Note that the data have been shifted vertically and in all cases $\Delta(T_0) = 0$ by definition. Δ_{CO} is determined from the increase of $\Delta(T)$ below the respective T_{CO}, i.e., $\Delta_{CO} = \sqrt{\Delta^2_{max} - \Delta^2(T_{CO})}$, as indicated by the double arrows and dashed lines in respective colors in Figure 5a. From our present transport results, we obtain $\Delta_{CO} = 430$ K for $(TMTTF)_2[AsF_6]_{0.7}[SbF_6]_{0.3}$.

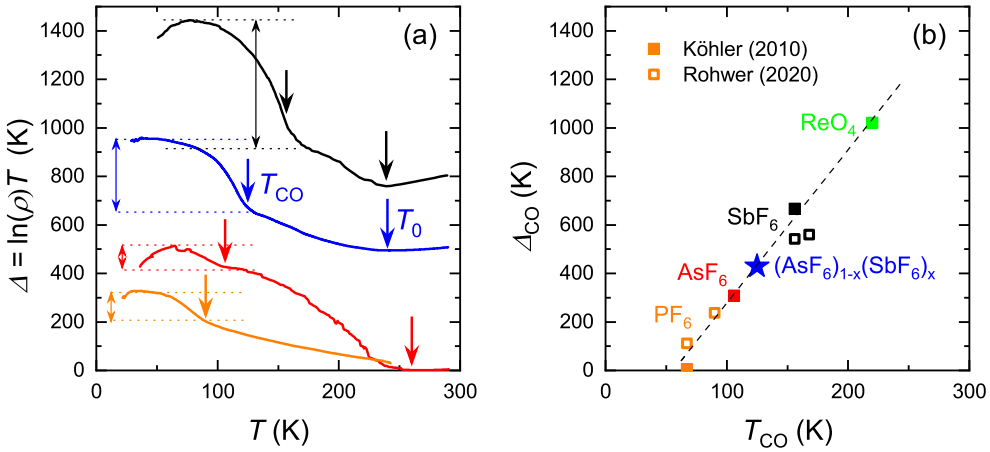

Figure 5. (**a**) Temperature-dependent energy gap of $(TMTTF)_2[AsF_6]_{1-x}[SbF_6]_x$ for $x = 0$ [37], 0.3, and 1 [37], and for deuterated $(TMTTF)_2PF_6$ with T_{CO}= 90 K [39]. The total gap size, measured by the resistivity, increases as Δ_{CO} adds up in quadrature $\Delta(T) = T \ln \rho = \sqrt{\Delta^2_{CO} + \Delta^2(T_{CO})}$ in the CO state. The increase from $\Delta(T_{CO})$ to Δ_{max} is indicated by double arrows and dashed lines in respective colors. The curves have been vertically shifted; by definition $\Delta(T_0) = 0$. (**b**) Δ_{CO} of $(TMTTF)_2[AsF_6]_{1-x}[SbF_6]_x$ (blue star) is plotted versus T_{CO} together with the data (solid squares) of $(TMTTF)_2X$ with $X = PF_6^-$, AsF_6^-, SbF_6^- and ReO_4^- [37]. Open squares indicate measurements on pristine and deuterated PF_6^- and SbF_6^- compounds [39]. The data follow an approximately linear relationship until Δ_{CO} vanishes for $T_{CO} \leq 60$ K. Alternatively, this *universal* behavior can be interpreted as a negative Δ_{CO} for $T_{CO} \to 0$.

In Figure 5b, we plot Δ_{CO} as a function of T_{CO} for the data shown in (a), i.e., $(TMTTF)_2[AsF_6]_{1-x}[SbF_6]_x$ with $x = 0.3$ (star) and PF_6^-, AsF_6^-, SbF_6^-, together with ReO_4^- (solid squares) [37]. Included are also additional datasets for pristine and deuterated compounds

from [39], indicated by the open squares. As we find, all data points fall on a *universal* line that yields $\Delta_{CO} = 0$ around $T_{CO} = 60$ K. It is tempting to relate this temperature scale with $D/k_B \approx 60$ K reported in Figure 8b of [14]. In that work, deuteration was found to contribute an energy D in quadrature to T_{CO}, suggesting that interactions between anions and the TMTTF donors via the hydrogen atoms interfere with the CO mechanism: T_{CO} is smaller in the protonated compounds compared to the heavier, less-mobile deuterium isotopes. Our results on $(TMTTF)_2[AsF_6]_{1-x}[SbF_6]_x$ provide an additional piece of evidence for the importance of anion-TMTTF interactions and motivate further research in this direction. More precise evaluation of the anion modes and vibrations of the methyl endgroups, possibly supplemented by calculations, may be a first step in this direction.

While assessing the *universal* behavior in Figure 5b, one could also consider that Δ_{CO} has a negative offset for $T_{CO} \to 0$, meaning that the repulsive interactions turn into attractive charge fluctuations as correlations diminish. This mechanism has been vividly discussed as a potential candidate for the pairing glue in the quasi-2D molecular superconductors nearby a CO instability [40–45]. This notion also calls for further scrutiny of the CO phenomenon by means of continuous correlation tuning, as presented here.

3.2. Charge Disproportionation Determined by Vibrational Spectroscopy

We investigate CO in $(TMTTF)_2[AsF_6]_{0.7}[SbF_6]_{0.3}$ in more detail by assessing the optical response of molecular vibrations in the midinfrared frequency range [1,38]. The charge-sensitive $\nu_{28}(b_{1u})$ mode probed for $E \parallel c$ exhibits a similar splitting in the CO phase ($T = 20$ K $< T_{CO}$) as in the two parent compounds (Figure 6). According to Equation (1), the separation of the two main peaks corresponds to the charge disproportionation 2δ between charge-rich and charge-poor molecular sites, which increases from $x = 0$ to $x = 1$. Overall, the ν_{28} mode for $x = 0.3$ very much resembles the spectrum of $x = 0$, in agreement with the chemical composition, placing the alloy closer to $(TMTTF)_2AsF_6$ in the phase diagram (Figure 1a). We also assessed the optical reflectivity parallel to the stacks ($E \parallel a$, see inset of Figure 6) and observe no significant activation of the ν_4 mode that is sensitive to tetramerization of the TMTTF molecules [1,36]. Therefore, we find no evidence for a spin-Peierls transition in $(TMTTF)_2[AsF_6]_{0.7}[SbF_6]_{0.3}$ based on our optical data, in line with the magnetic susceptibility measurements shown in Figure 3. The suppression of the spin-Peierls state is in agreement with pressure-dependent experiments on $(TMTTF)_2SbF_6$ and $(TMTTF)_2AsF_6$, where antiferromagnetism rapidly replaces the spin-gapped phase [6,35,36].

Figure 7a presents the optical conductivity of the $\nu_{28}(b_{1u})$ vibration in $(TMTTF)_2[AsF_6]_{0.7}[SbF_6]_{0.3}$ for various temperatures above and below T_{CO}. Consistent with our transport results in Figure 4, the line exhibits a splitting at $T \leq 120$ K. For a quantitative analysis, we determined the charge disproportionation 2δ from the resonance frequencies of the peak splitting according to Equation (1), as shown in panels (b) and (c). On first glance, 2δ exhibits a similar mean-field-like increase upon cooling below T_{CO}. While the transition temperature is higher than in the parent compound $(TMTTF)_2AsF_6$ [1,12], the charge disproportionation reaches a rather similar value of $2\delta = 0.21e$ in the limit $T \to 0$.

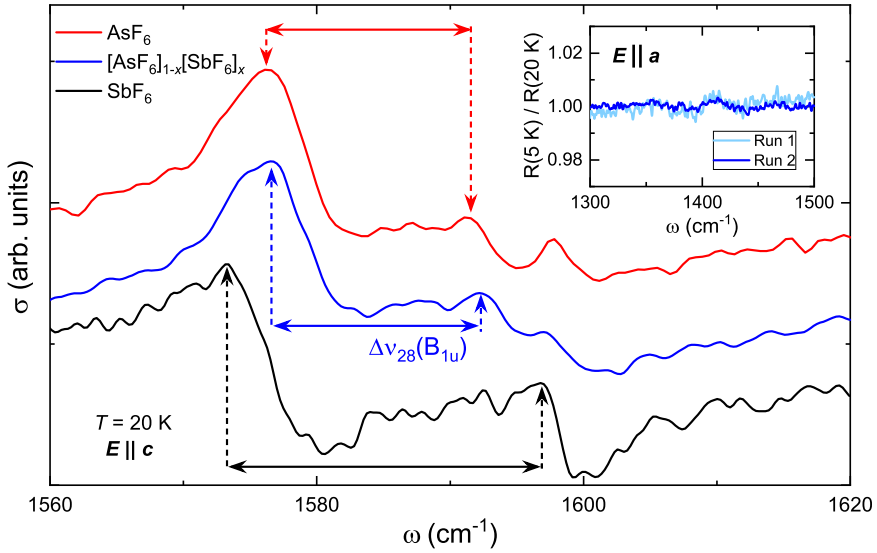

Figure 6. The ν_{28} mode in $(TMTTF)_2[AsF_6]_{1-x}[SbF_6]_x$ with $x = 0.3$ is plotted at $T = 20$ K and compared to the parent compounds $(TMTTF)_2SbF_6$ and $(TMTTF)_2AsF_6$ [1,12]. The overall low-temperature spectrum is very similar for $x = 0$ and 0.3, with a smaller line splitting $\Delta\nu_{28}$ than for $x = 1$. For better comparison of the peaks, the data were scaled and shifted by a vertical offset. Inset: Comparing the reflectivity for $E \parallel a$ at 5 K and 20 K yields no enhancement of the ν_4 mode [1,36]; two distinct measurement runs of the same $(TMTTF)_2[AsF_6]_{1-x}[SbF_6]_x$ sample are shown. The absence of tetramerization indicates that the spin-Peierls phase is suppressed for a substitution $x = 0.3$, which is taken into account in Figure 1a.

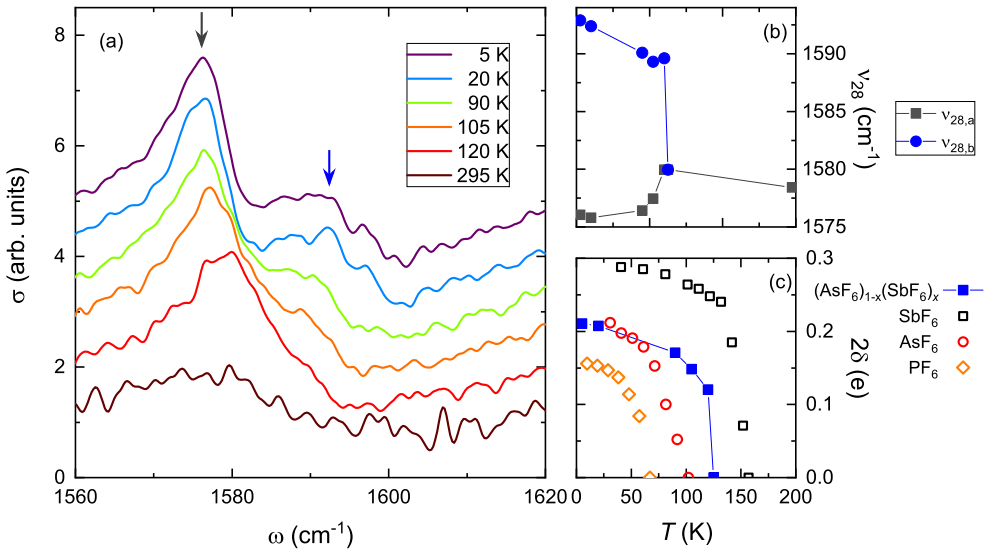

Figure 7. (**a**) Temperature dependence of the ν_{28} mode in $(TMTTF)_2[AsF_6]_{1-x}[SbF_6]_x$ for $x = 0.3$; the spectrum is very similar to $(TMTTF)_2AsF_6$ [1,12]. While the charge-rich, low-frequency peak can be identified clearly, the charge-poor, high-frequency peak is spread out more broadly. The data have been shifted vertically. (**b**) Peak frequencies from (**a**). (**c**) The charge disproportionation below $T_{CO} = 120$ K approaches a similar value towards $T \to 0$ as for $(TMTTF)_2AsF_6$. The temperature evolution of 2δ upon CO is compared among $(TMTTF)_2X$ with $X = PF_6^-$, AsF_6^- and SbF_6^- (data taken from [1,12]).

4. Discussion and Outlook

The dichotomy of T_{CO} (and Δ_{CO}) and $2\delta(T = 0)$, where the former increases upon anion substitution x in $(TMTTF)_2[AsF_6]_{1-x}[SbF_6]_x$ while the latter remains unchanged (see Figure 6), is surprising in view of the monotonous increase of both quantities in the

stoichiometric compounds. A priori, from the empirical trend (see Figure 4 in [14]), one would expect a 20% larger value of 2δ based on T_{CO}= 120 K. Possibly, the molecular charge arranges according to the closest anion: 2δ is larger nearby SbF_6^- anions and smaller around AsF_6^-, where the latter constitute the majority of anions. The local increase of charge disproportionation around SbF_6^- sites can be gradual as it depends on the structural extent of the lattice distortion, resulting in a distribution of 2δ. Indeed, the ν_{28} lines are broadened and more smeared in the spectrum of $x = 0.3$ compared to $x = 0$ (Figure 6). Note that, while our spectroscopic data are consistent with a microscopic modulation of the local CO amplitude, our transport data reveal only a single T_{CO} = 120 K, and the crystal as a whole does not exhibit two transitions. Structural phase separation is further ruled out as χ_s (Figure 3) does not exhibit a distinct drop at $T_{SP} = 13$ K expected for volume fractions of pure $(TMTTF)_2AsF_6$. This shows that the macroscopic CO transition is a 3D bulk phenomenon that requires substantial coupling among the one-dimensional TMTTF chains—through/with the anions. To that end, the abovementioned TMTTF–anion interactions via the hydrogen atoms are crucial ingredients to CO, opposite to the original notions about a *structureless* transition. Certainly, the microscopic charge disproportionation should be studied in more detail by assessing different values of the substitution x and by complementary methods, such as NMR or other local probes. Magnetic resonance measurements are also required to investigate the magnetic ground state: studying the borderland of antiferromagnetic and spin-Peierls phases is of particular interest to the field of frustrated magnetism and quantum spin liquids [46].

Using partial substitution of the anions, it will be interesting to inspect the length scales of long-range correlations and short-range CO modulations and associated disorder effects—in particular in the deuterated compounds where CO is affected from a change in TMTTF–anion coupling [14,39]. In addition, the interplay of CO and anion order can be studied via mixing of octahedral and tetrahedral anions, which can possibly stabilize novel forms of structural order at commensurate stoichiometries. We further suggest to partially introduce anions, that are not regularly used for single crystal growth, into "established" systems which provides another knob to tune through unexplored phase space.

Moreover, it is intriguing to compare the continuous correlation tuning methods of physical pressure and partial chemical substitution. While the former truly modifies the interactions locally, in the latter case, the microscopic mixture of distinct constituents yields a change of correlation strength on a macroscopic level, i.e., "on average". We expect fundamental differences between (super)conducting systems with itinerant charge carriers in the vicinity of the Mott transition [24,26–29,31] and the fully insulating Fabre salts inspected here. Clearly, partial chemical substitution is a powerful tool that enables us to put *new spin on metal-insulator transitions*.

5. Summary

We report transport and optical spectroscopy experiments on partially substituted $(TMTTF)_2[AsF_6]_{1-x}[SbF_6]_x$ with $x = 0.3$, which is equivalent to "negative" pressure applied to $(TMTTF)_2AsF_6$. The transition temperature $T_{CO} = 120$ K and charge gap $\Delta_{CO} = 430$ K indicate that this alloy is between the parent compounds $(TMTTF)_2AsF_6$ and $(TMTTF)_2SbF_6$, a little closer to the former in agreement with the stoichiometry. This demonstrates the powerful capabilities of partial anion substitution for continuous bandwidth tuning. Upon plotting Δ_{CO} as a function of T_{CO} for various $(TMTTF)_2X$ salts exhibiting CO, all data points fall on a universal line. We find that Δ_{CO} vanishes around $T_{CO} = 60$ K—a value similar to the contribution to CO upon deuteration ($D \approx 60$ K reported in [14]). While the macroscopic CO transition and its underlying electronic correlation strength are tuned continuously, our measurements utilizing the local probe of vibrational spectroscopy indicate that the charge disproportionation adheres to the closest anion on a microscopic level, yielding a short-range modulation of the CO amplitude around the substituent sites.

Author Contributions: Conceptualization and supervision, A.P. and M.D.; crystal growth, G.U.; transport and optical investigation and analysis, A.P., D.D. and S.E.; magnetic characterization, O.I. and V.M.; writing and editing, A.P. All authors have read and agreed to the published version of the manuscript.

Funding: Deutsche Forschungsgemeinschaft.

Data Availability Statement: The authors declare that the data supporting the findings of this study are available within the paper. Further information can be provided by A.P. or M.D.

Acknowledgments: The project was supported by the Deutsche Forschungsgemeinschaft (DFG). The authors acknowledge TU Wien Bibliothek for financial support through its Open Access Funding Program.

Conflicts of Interest: The authors declare no conflicts of interest.

References

1. Dressel, M.; Dumm, M.; Knoblauch, T.; Masino, M. Comprehensive Optical Investigations of Charge Order in Organic Chain Compounds $(TMTTF)_2X$. *Crystals* **2012**, *2*, 528–578. [CrossRef]
2. Fukuyama, H. Physics of Molecular Conductors. *J. Phys. Soc. Jpn.* **2006**, *75*, 51001. [CrossRef]
3. Seo, H.; Merino, J.; Yoshioka, H.; Ogata, M. Theoretical Aspects of Charge Ordering in Molecular Conductors. *J. Phys. Soc. Jpn.* **2006**, *75*, 51009. [CrossRef]
4. Chow, D.S.; Zamborszky, F.; Alavi, B.; Tantillo, D.J.; Baur, A.; Merlic, C.A.; Brown, S.E. Charge Ordering in the TMTTF Family of Molecular Conductors. *Phys. Rev. Lett.* **2000**, *85*, 1698–1701. [CrossRef]
5. Zamborszky, F.; Yu, W.; Raas, W.; Brown, S.E.; Alavi, B.; Merlic, C.A.; Baur, A. Competition and coexistence of bond and charge orders in $(TMTTF)_2AsF_6$. *Phys. Rev. B* **2002**, *66*, 81103. [CrossRef]
6. Yu, W.; Zhang, F.; Zamborszky, F.; Alavi, B.; Baur, A.; Merlic, C.A.; Brown, S.E. Electron-lattice coupling and broken symmetries of the molecular salt $(TMTTF)_2SbF_6$. *Phys. Rev. B* **2004**, *70*, 121101. [CrossRef]
7. Dumm, M.; Salameh, B.; Abaker, M.; Montgomery, L.K.; Dressel, M. Magnetic and optical studies of spin and charge ordering in $(TMTTF)_2AsF_6$. *J. Phys. IV* **2004**, *114*, 57–60. [CrossRef]
8. Dumm, M.; Abaker, M.; Dressel, M. Mid-infrared response of charge-ordered quasi-1D organic conductors $(TMTTF)_2X$. *J. Phys. IV* **2005**, *131*, 55–58. [CrossRef]
9. Dumm, M.; Abaker, M.; Dressel, M.; Montgomery, L.K. Charge Order in $(TMTTF)_2PF_6$ Investigated by Infrared Spectroscopy. *J. Low Temp. Phys.* **2006**, *142*, 613–616. [CrossRef]
10. Pashkin, A.; Dressel, M.; Ebbinghaus, S.; Hanfland, M.; Kuntscher, C. Pressure-induced structural phase transition in the Bechgaard-Fabre salts. *Synth. Met.* **2009**, *159*, 2097–2100. [CrossRef]
11. Pashkin, A.; Dressel, M.; Hanfland, M.; Kuntscher, C.A. Deconfinement transition and dimensional crossover in the Bechgaard-Fabre salts: Pressure- and temperature-dependent optical investigations. *Phys. Rev. B* **2010**, *81*, 125109. [CrossRef]
12. Knoblauch, T.; Dressel, M. Charge disproportionation in $(TMTTF)_2X$ ($X = PF_6$, AsF_6 and SbF_6) investigated by infrared spectroscopy. *Phys. Status Solidi C* **2012**, *9*, 1158–1160. [CrossRef]
13. Oka, Y.; Matsunaga, N.; Nomura, K.; Kawamoto, A.; Yamamoto, K.; Yakushi, K. Charge Order in $(TMTTF)_2TaF_6$ by Infrared Spectroscopy. *J. Phys. Soc. Jpn.* **2015**, *84*, 114709. [CrossRef]
14. Pustogow, A.; Peterseim, T.; Kolatschek, S.; Engel, L.; Dressel, M. Electronic correlations versus lattice interactions: Interplay of charge and anion orders in $(TMTTF)_2X$. *Phys.Rev. B* **2016**, *94*, 195125. [CrossRef]
15. Rösslhuber, R.; Rose, E.; Ivek, T.; Pustogow, A.; Breier, T.; Geiger, M.; Schrem, K.; Untereiner, G.; Dressel, M. Structural and Electronic Properties of $(TMTTF)_2X$ Salts with Tetrahedral Anions. *Crystals* **2018**, *8*, 121. [CrossRef]
16. Parkin, S.S.P.; Coulon, C.; Jérome, D.; Fabre, J.M.; Giral, L. Substitution of TMTSeF with TMTTF in $(TMTSeF)_2ClO_4$: High pressure studies. *J. Phys. France* **1983**, *44*, 603–607. [CrossRef]
17. Ilakovac, V.; Ravy, S.; Pouget, J.P.; Lenoir, C.; Boubekeur, K.; Batail, P.; Babic, S.D.; Biskup, N.; Korin-Hamzic, B.; Tomic, S.; Bourbonnais, C. Enhanced charge localization in the organic alloys $[(TMTSF)_{1-x}(TMTTF)_x]_2ReO_4$. *Phys. Rev. B* **1994**, *50*, 7136–7139. [CrossRef]
18. Tomic, S.; Auban-Senzier, P.; Jérome, D. Charge localization in $[(TMTTF)_{0.5}(TMTSF)_{0.5}]_2ReO_4$: A pressure study. *Synth. Met.* **1999**, *103*, 2197–2198. [CrossRef]
19. Naito, T.; Miyamoto, A.; Kobayashi, H.; Kato, R.; Kobayashi1, A. Superconducting Transition Temperature of the Organic Alloy System. κ-$[(BEDT\text{-}TTF)_{1-x}(BEDT\text{-}STF)_x]_2Cu[N(CN)_2]Br$. *Chem. Lett.* **1992**, *21*, 119–122. [CrossRef]
20. Kawamoto, A.; Taniguchi, H.; Kanoda, K. Superconductor-Insulator Transition Controlled by Partial Deuteration in BEDT-TTF Salt. *J. Am. Chem. Soc.* **1998**, *120*, 10984–10985. [CrossRef]
21. Sasaki, J.; Kawamoto, A.; Kumagai, K.I. Magnetic Properties of the alloy of κ-$(BEDT\text{-}TTF)_{2(1-X)}(BEDSe\text{-}TTF)_{2X}Cu[N(CN)_2]Br$. *Synth. Met.* **2003**, *137*, 1249–1250. [CrossRef]
22. Sushko, Y.V.; Leontsev, S.O.; Korneta, O.B.; Kawamoto, A. SQUID-magnetometry study of the P-T phase diagram of κ-$[(BEDT\text{-}TTF)_{1-x}(BEDSe\text{-}TTF)_x]_2Cu[N(CN)_2]Br$. *J. Low Temp. Phys.* **2006**, *142*, 563–566. [CrossRef]

23. Kobayashi, T.; Ihara, Y.; Kawamoto, A. Modification of local electronic state by BEDT-STF doping to κ-(BEDT-TTF)$_2$Cu[N(CN)$_2$]Br salt studied by ^{13}C NMR spectroscopy. *Phys. Rev. B* **2016**, *93*, 94515. [CrossRef]
24. Saito, Y.; Minamidate, T.; Kawamoto, A.; Matsunaga, N.; Nomura, K. Site-specific ^{13}C NMR study on the locally distorted triangular lattice of the organic conductor κ-(BEDT-TTF)$_2$Cu$_2$(CN)$_3$. *Phys. Rev. B* **2018**, *98*, 205141. [CrossRef]
25. Yesil, E.; Imajo, S.; Nomoto, T.; Yamashita, S.; Akutsu, H.; Nakazawa, Y. Variation of Electronic Heat Capacity of κ-(BEDT-TTF)$_2$Cu[N(CN)$_2$]Br Induced by Partial Substitution of Donor Layers. *J. Phys. Soc. Jpn.* **2020**, *89*, 73701. [CrossRef]
26. Pustogow, A.; Saito, Y.; Löhle, A.; Sanz Alonso, M.; Kawamoto, A.; Dobrosavljević, V.; Dressel, M.; Fratini, S. Rise and fall of Landau's quasiparticles while approaching the Mott transition. *Nat. Commun.* **2021**, *12*, 1571. [CrossRef]
27. Pustogow, A.; Rösslhuber, R.; Tan, Y.; Uykur, E.; Böhme, A.; Wenzel, M.; Saito, Y.; Löhle, A.; Hübner, R.; Kawamoto, A.; et al. Low-temperature dielectric anomaly arising from electronic phase separation at the Mott insulator-metal transition. *NPJ Quantum Mater.* **2021**, *6*, 9. [CrossRef]
28. Saito, Y.; Rösslhuber, R.; Löhle, A.; Sanz Alonso, M.; Wenzel, M.; Kawamoto, A.; Pustogow, A.; Dressel, M. Chemical tuning of molecular quantum materials κ-[(BEDT-TTF)$_{1-x}$(BEDT-STF)$_x$]$_2$Cu$_2$(CN)$_3$: From the Mott-insulating quantum spin liquid to metallic Fermi liquid. *J. Mater. Chem. C* **2021**, *9*, 10841–10850. [CrossRef]
29. Saito, Y.; Löhle, A.; Kawamoto, A.; Pustogow, A.; Dressel, M. Pressure-Tuned Superconducting Dome in Chemically-Substituted κ-(BEDT-TTF)$_2$Cu$_2$(CN)$_3$. *Crystals* **2021**, *11*, 817. [CrossRef]
30. Joo, N.; Auban-Senzier, P.; Pasquier, C.R.; Jérome, D.; Bechgaard, K. Impurity-controlled superconductivity/spin density wave interplay in the organic superconductor: (TMTSF)$_2$ClO$_4$. *EPL* **2005**, *72*, 645–651. [CrossRef]
31. Faltermeier, D.; Barz, J.; Dumm, M.; Dressel, M.; Drichko, N.; Petrov, B.; Semkin, V.; Vlasova, R.; Meźière, C.; Batail, P. Bandwidth-controlled Mott transition in $\kappa-$(BEDT$-$TTF)$_2$Cu[N(CN)$_2$]Br$_x$Cl$_{1-x}$: Optical studies o. *Phys. Rev. B* **2007**, *76*, 165113. [CrossRef]
32. Dumm, M.; Faltermeier, D.; Drichko, N.; Dressel, M.; Mézière, C.; Batail, P. Bandwidth-controlled Mott transition in κ-(BEDT-TTF)$_2$Cu[N(CN)$_2$]Br$_x$Cl$_{1-x}$: Optical studies of correlated carriers. *Phys. Rev. B* **2009**, *79*, 195106. [CrossRef]
33. Yoshida, Y.; Maesato, M.; Tomeno, S.; Kimura, Y.; Saito, G.; Nakamura, Y.; Kishida, H.; Kitagawa, H. Partial Substitution of Ag(I) for Cu(I) in Quantum Spin Liquid κ-(ET)$_2$Cu$_2$(CN)$_3$, Where ET Is Bis(ethylenedithio)tetrathiafulvalene. *Inorg. Chem.* **2019**, *58*, 4820–4827. [CrossRef]
34. Kitou, S.; Zhang, L.; Nakamura, T.; Sawa, H. Complex changes in structural parameters hidden in the universal phase diagram of the quasi-one-dimensional organic conductors $(\mathrm{TMTTF})_2X$ (X = NbF$_6$, AsF$_6$, PF$_6$, and Br). *Phys. Rev. B* **2021**, *103*, 184112. [CrossRef]
35. Yu, W.; Zamborszky, F.; Alavi, B.; Baur, A.; Merlic, C.A.; Brown, S.E. Influence of charge order on the ground states of TMTTF molecular salts. *J. Phys. IV France* **2004**, *114*, 35–40. [CrossRef]
36. Voloshenko, I.; Herter, M.; Beyer, R.; Pustogow, A.; Dressel, M. Pressure-dependent optical investigations of Fabre salts in the charge-ordered state. *J. Phys. Condens. Matter* **2017**, *29*, 115601. [CrossRef]
37. Köhler, B.; Rose, E.; Dumm, M.; Untereiner, G.; Dressel, M. Comprehensive transport study of anisotropy and ordering phenomena in quasi-one-dimensional $(\mathrm{TMTTF})_2X$ salts (X = PF$_6$, AsF$_6$, SbF$_6$, BF$_4$, ClO$_4$, ReO$_4$). *Phys. Rev. B* **2011**, *84*, 035124. [CrossRef]
38. Meneghetti, M.; Bozio, R.; Zanon, I.; Pecile, C.; Ricotta, C.; Zanetti, M. Vibrational behavior of molecular constituents of organic superconductors: TMTSF, its radical cation and the sulphur analogs TMTTF and TMTTF$^+$. *J. Chem. Phys.* **1984**, *80*, 6210. [CrossRef]
39. Rohwer, A.; Dressel, M.; Nakamura, T. Deuteration Effects on the Transport Properties of $(\mathrm{TMTTF})_2X$ Salts. *Crystals* **2020**, *10*, 1085. [CrossRef]
40. Merino, J.; McKenzie, R.H. Superconductivity Mediated by Charge Fluctuations in Layered Molecular Crystals. *Phys. Rev. Lett.* **2001**, *87*, 237002. [CrossRef]
41. Drichko, N.; Dressel, M.; Kuntscher, C.; Pashkin, A.; Greco, A.; Merino, J.; Schlueter, J. Electronic properties of correlated metals in the vicinity of a charge-order transition: Optical spectroscopy of α-(BEDT-TTF)$_2$MHg(SCN)$_4$ (M = NH$_4$, Rb, Tl). *Phys. Rev. B* **2006**, *74*, 235121. [CrossRef]
42. Kaiser, S.; Dressel, M.; Sun, Y.; Greco, A.; Schlueter, J.A.; Gard, G.L.; Drichko, N. Bandwidth Tuning Triggers Interplay of Charge Order and Superconductivity in Two-Dimensional Organic Materials. *Phys. Rev. Lett.* **2010**, *105*, 206402. [CrossRef]
43. Pustogow, A.; Saito, Y.; Rohwer, A.; Schlueter, J.A.; Dressel, M. Coexistence of charge order and superconductivity in $\beta''-(\mathrm{BEDT}-\mathrm{TTF})_2\mathrm{SF}_5\mathrm{CH}_2\mathrm{CF}_2\mathrm{SO}_3$. *Phys. Rev. B* **2019**, *99*, 140509. [CrossRef]
44. Imajo, S.; Akutsu, H.; Akutsu-Sato, A.; Morritt, A.L.; Martin, L.; Nakazawa, Y. Effects of electron correlations and chemical pressures on superconductivity of β''-type organic compounds. *Phys. Rev. Res.* **2019**, *1*, 33184. [CrossRef]
45. Imajo, S.; Akutsu, H.; Kurihara, R.; Yajima, T.; Kohama, Y.; Tokunaga, M.; Kindo, K.; Nakazawa, Y. Anisotropic Fully Gapped Superconductivity Possibly Mediated by Charge Fluctuations in a Nondimeric Organic Complex. *Phys. Rev. Lett.* **2020**, *125*, 177002. [CrossRef]
46. Balents, L. Spin liquids in frustrated magnets. *Nature* **2010**, *464*, 199–208. [CrossRef]